Jordan Journal of Civil Engineering, Volume **20**, No. **3**, **2026**
DOI: https://doi.org/10.14525/JJCE.v20i3.05

Jordan Journal of Civil Engineering

Journal homepage: https://jjce.just.edu.jo

Effect of the Flexibility of Superstructure on the Displacement of Isolation Systems with Single Friction Pendulum Bearings

Nam Van Nguyen[1)*], Nhan Dinh Dao[2)], Hoang D. Nguyen[3)], Thanh-Truc Nguyen[4)]

[1)] *Faculty of Civil Engineering, Industrial University of Ho Chi Minh City, Vietnam.*
[2] *Institute of International Education, University of Architecture Ho Chi Minh City, Vietnam.*
[3] *Department of Civil and Environmental Engineering, Faculty of Engineering, University of Alberta, Edmonton, Alberta, Canada T6G 1H9.*
[4] *Faculty of Civil Engineering, Mien Tay Construction University, Vietnam.*
[*] *Corresponding Author. Email: nguyenvannam@iuh.edu.vn*

ARTICLE INFO

Article History:
Received: 10/7/2025
Accepted: 1/1/2026

ABSTRACT

Accurately predicting displacement is crucial in the design of isolation systems. Rigid mass models, which neglect the superstructure's flexibility, are commonly used for this purpose due to their simplicity. However, this assumption may compromise accuracy by neglecting the superstructure's flexibility. This study investigates the validity of the rigid mass model for isolation systems with single friction pendulums by comparing its displacement predictions to those of flexible superstructure models. A comprehensive analysis was conducted on 1720 isolation system models subjected to 245 ground motion records, including both pulse-like and no-pulse motions. Statistical results show that when the stiffness ratio, defined as the ratio of the isolation system's effective period to the superstructure's fundamental period, exceeds certain thresholds, the displacement of the isolation system becomes largely independent of the superstructure's flexibility. Conversely, at lower stiffness ratios, the displacement exhibits significant variability, highlighting the complex interactions between the superstructure and the isolation system. Additionally, the findings reveal that pulse-like ground motions result in lower displacement variability compared to non-pulse motions, and that taller buildings are more sensitive to the effects of superstructure flexibility, despite sharing the same fundamental period.

Keywords: Isolation systems, Peak displacement, Friction bearings, Earthquake design.

INTRODUCTION

Seismic isolation offers an effective approach to protect buildings from earthquakes by decoupling the superstructure from the ground motion. Among the various isolation techniques, friction-based isolation systems have gained prominence due to their simplicity, effectiveness, and ability to dissipate energy through sliding friction. These systems typically employ spherical sliding interfaces with defined friction coefficients to provide flexibility to isolated buildings. While the performance of friction isolation systems has been extensively studied under the assumption of a rigid superstructure, real-world buildings exhibit varying degrees of flexibility, influenced by their height, structural configuration, and material properties. Understanding how this flexibility affects the displacement response of friction isolation systems is critical for optimizing their design, ensuring their reliability across a range of seismic scenarios, and

selecting appropriate models for analysis.

According to Kelly (1986) and Buckle and Mayes (1990), the concept of seismic isolation dates back to early proposals by practitioners, such as Jacob Bechtold in 1906 and Calantarients in 1909, who suggested separating buildings from the ground using rollers or sliding layers. Modern developments, however, were attributed to the work of researchers, like Kelly (1986), who formalized the theoretical framework for base isolation, and Mokha et al. (1990), who advanced the understanding of friction pendulum systems. Since then, a vast number of studies have been carried out to understand the isolation approach, as well as to enhance its application.

While detailed superstructure models are necessary for accurately evaluating superstructure response or modeling special cases, like liquid storage tanks (Jamalvandi & Amiri, 2021; Jing & Zhang, 2024), many seismic isolation studies simplify the superstructure as a rigid mass. This assumption is generally reasonable for low-rise, stiff buildings. Dicleli and Buddaram (2007) employed the rigid mass superstructure model to investigate the accuracy of an equivalent linear force procedure in predicting the non-linear time history responses of isolation systems. Katsaras et al. (2008) and Cardone et al. (2015) used the rigid mass model to investigate the restoring capability of both single friction pendulum systems and lead rubber bearing with bilinear behavior systems. Fadi and Constantinou (2010) utilized the single mass model to assess simplified analysis methods for structures isolated by triple friction pendulum bearings. Dao et al. (2020) used the rigid mass model to develop statistical equations for predicting the peak displacement of isolation systems. Nguyen et al. (2022) made use of the single mass model to generate numerical data to develop machine learning (ML) models to predict the peak displacement of isolation systems. Alici et al. (2024) employed the single mass model to develop charts to predict the peak displacement of isolation systems. Dao (2025, 2026) utilized rigid superstructure assumption to build ML models and simple equations to predict the peak displacement of isolation systems.

As isolation systems have been applied to increasingly taller and more flexible structures, the validity of rigid superstructures assumption has come under scrutiny. Many researchers have tested this assumption, but the conclusion is controversial. While some researchers, such as Kulkarni and Jangid (2002, 2003), Alhan and Surmeli (2011), and Bhagat and Wijeyewickrema (2017), concluded that the flexibility of the superstructure has little effect on the displacement of an isolation system, other researchers have highlighted the influence of superstructure flexibility on isolation system performance. For instance, Kanbir et al. (2020) observed that neglecting the flexibility of the superstructure can overestimate the displacement of an isolation system. Zhong et al. (2023) proposed a multivariable probabilistic equation to predict the peak displacement demand of friction isolation bearings in isolated bridge systems under pulse-like ground motions. According to the equation, the superstructure's flexibility plays an important role in predicting the displacement.

Notably, modern design codes, such as ASCE 7-22 (ASCE, 2022) and Eurocode 8 (CEN, 2004), allow using an equivalent force procedure in which the superstructure is considered rigid to predict the peak displacement of an isolation system when the effective period of the isolation system exceeds three times the period of the base-fixed superstructure. This provision implies that if the ratio between the effective period of the isolation system to the period of the base-fixed superstructure is larger than a threshold, then the superstructure's flexibility can be neglected. However, to the best of our knowledge, the thorough investigation of this threshold has not been carried out.

To provide a clear picture of the effect of the superstructure's flexibility on the peak displacement of an isolation system with single friction pendulum (SFP) bearings, this study investigated the effect through an extensive numerical simulation. The analysis encompasses 40 isolation systems with varying friction coefficients and post-yield periods, applied to a rigid mass model and three building groups representing low-rise (1-story), medium-rise (5-story), and high-rise (9-story) structures. Each building group includes 14 structural systems with fundamental periods ranging from 1/10 to 1/10 times the isolation system's effective period. Subjected to 245 ground motion pairs, including both pulse-like and no-pulse motions, the resulting 421,400 non-linear dynamic analyses provide a comprehensive dataset to evaluate displacement trends. By examining the displacement ratio as a function of the period ratio, ground motion type, and building height, this investigation seeks to offer new insights into the

design and performance of friction isolation systems in flexible superstructures, building on the foundational work of prior researchers while extending the scope to a broader parametric space.

Unlike previous works that were limited to a few dozen records or a narrow parametric range, the present study provides the systematic evaluation specifically targeted at SFP-isolated buildings, using an unprecedented database of 421,400 bidirectional non-linear response-history analyses that simultaneously vary isolation properties, superstructure height and stiffness, and ground-motion characteristics. This enables statistical identification of the conditions under which the conventional rigid-superstructure idealization remains valid for predicting peak isolator displacement in frictional systems, thereby offering practical guidance that is not available from previous investigations.

STRUCTURAL MODELING

This study employed bidirectional shear frame structure models to investigate the effect of the superstructure's flexibility on the peak displacement of an isolation system. The bearings were modeled by a bidirectional coupling plasticity element, and the superstructure was modeled by two orthogonal shear frames. A non-linear time-history analysis of the model subjected to ground motions was performed using the OpenSees simulation software. The detailed modeling approach is presented next.

Modeling the Isolation System

The backbone curve of the hysteresis behavior in a horizontal direction of an SFP with a constant sliding friction coefficient μ subjected to a constant vertical load W is shown in Figure 1. The development of this backbone curve can easily be found in the literature (Constantinou et al., 1993). In this graph, the horizontal axis represents the horizontal displacement u_b of the bearing, and the vertical axis represents the corresponding horizontal force F_b. Key parameters postulating the behavior of the bearing include the sliding friction coefficient μ, which determines the yielding force, and the radius R, which determines the post-yield slope, of its concave surface. The displacement limit of the bearing is determined by its size, which is usually disregarded if the peak displacement of the bearing is smaller than this limit.

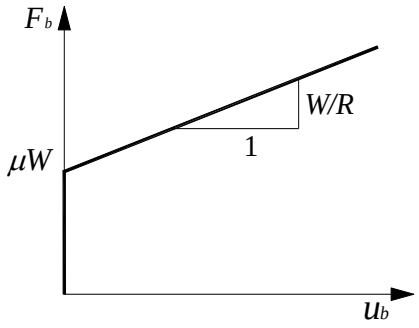

Figure 1. The unidirectional backbone curve of a single friction pendulum bearing

In practice, the sliding surface of an SFP is usually made of polytetrafluoroethylene. The sliding friction coefficient of this material depends on sliding velocity, surface pressure, and temperature (Mokha, 1988; Dolce et al., 2005; Quaglini et al., 2012). Detailed analysis of isolation systems should include these effects. However, this study assumed that the sliding friction coefficient remains unchanged for the purposes of a general investigation. This assumption has been adopted in many studies (van de Lindt & Jiang, 2013; Peng et al. 2018; Xu et al., 2019). It is also noted that a past study by Nhan and Ai (2020) has proposed equivalent constant friction coefficient models for friction bearings to obtain reasonable results compared to the results from the variable friction coefficient models. These results allow using a constant friction coefficient model that yields a peak displacement comparable to the peak displacement analyzed from a variational friction model.

Due to the friction effect and the dependency of the restoring force on the vertical load, the horizontal response of an SFP depends on its vertical load. This effect implies that the variation of the vertical load caused by the overturning effect and the vertical vibration of the isolated building can alter the horizontal response of the system. However, many past studies have shown that this phenomenon has a small effect on the peak displacement of an isolation system (Fenz & Constantinou, 2008; Cilsalar & Constantinou, 2017; Zhong et al., 2023; Kim & Constantinou, 2024). When this phenomenon is neglected, the hysteretic response of the bearing at its static load due to gravity can be used for the dynamic analysis. In this case, the whole isolation system with identical bearings can be lumped into a single element the friction coefficient and radius of which equal those of the individual bearing, and the vertical load equals the total weight of the isolated building (W).

For convenience, the normalized behavior, which equals the actual behavior divided by the vertical load, is usually employed to represent the behavior of an isolation system. The normalized backbone curve is obtained by dividing the backbone curve in Figure 1 by W.

Modeling the Superstructure

A common approach to include the superstructure's flexibility in analyzing the response of isolated buildings is to model the superstructure as a shear frame structure (Kulkarni & Jangid, 2002; Alhan & Surmeli, 2011; Dao et al., 2019). Dao et al. (2019) showed that this modeling approach yields a reasonable prediction for the isolation system's peak displacement of a tested full-scale building isolated with triple friction pendulum bearings. A procedure for calculating stories' shear stiffness from the superstructure's modal information was proposed in that research. Accordingly, the shear stiffness k_i of story i ($i = \overline{1,N}$, where N is the number of stories of the building) can be calculated from the story masses m_i, fundamental circular frequency ω_1, and fundamental mode shape $\{\Phi\}_1 = \{\phi_{11}, \phi_{21}, \dots, \phi_{N1}\}^T$ of the building, as follows:

$$k_N = \frac{\omega_1^2 m_N \phi_{N1}}{\phi_{N1} - \phi_{(N-1)1}} \tag{1}$$

$$k_i = \frac{\omega_1^2 m_i \phi_{i1} + k_{i+1}\left(\phi_{(i+1)1} - \phi_{i1}\right)}{\phi_{i1} - \phi_{(i-1)1}}, \text{for } i = N-1, N-2, \dots, 2 \tag{2}$$

$$k_1 = \frac{\omega_1^2 m_1 \phi_{11} + k_2(\phi_{21} - \phi_{11})}{\phi_{11}} \tag{3}$$

Each building's modal information depends on the dynamic properties of its structural system. This study assumed that the fundamental mode shape of a fixed-base superstructure is linearly distributed with story number and identical in any horizontal direction. The fundamental circular frequency was computed from the fundamental period T_1, which was assumed to be a factor of the effective period of the isolation system and will be discussed later.

An isolated structure is expected to experience minor damage during earthquakes. Therefore, the non-linear behavior of the superstructure was excluded in this investigation.

The projection of the governing equation of the system into a horizontal direction is:

$$[M]\{\ddot{u}\} + (\alpha_M[M] + \alpha_K[K]_C)\{\dot{u}\} + [K]_s\{u\} + \{F\}_n = -[M]\{i\}\ddot{u}_g \tag{4}$$

where:

$\{u\} = \{u_b, u_1, \dots, u_N\}$ = displacement vector.

$[M]$ = mass matrix.

$$[M] = \begin{bmatrix} m_b & 0 & 0 & \vdots & 0 \\ 0 & m_1 & 0 & \vdots & 0 \\ 0 & 0 & m_2 & \vdots & 0 \\ \dots & \dots & \dots & \ddots & \dots \\ 0 & 0 & 0 & \vdots & m_N \end{bmatrix} \tag{5}$$

$[K]_C$ = matrix for computing the stiffness proportional component of the damping matrix.

$$[K]_C = \begin{bmatrix} k_b + k_1 & -k_1 & 0 & \vdots & 0 \\ -k_1 & k_1 + k_2 & -k_2 & \vdots & 0 \\ 0 & -k_2 & k_2 + k_3 & \vdots & 0 \\ \dots & \dots & \dots & \ddots & \dots \\ 0 & 0 & 0 & \vdots & k_N \end{bmatrix} \tag{6}$$

$[K]_s$ = linear stiffness matrix.

$$[K]_s = \begin{bmatrix} k_1 & -k_1 & 0 & \vdots & 0 \\ -k_1 & k_1 + k_2 & -k_2 & \vdots & 0 \\ 0 & -k_2 & k_2 + k_3 & \vdots & 0 \\ \dots & \dots & \dots & \ddots & \dots \\ 0 & 0 & 0 & \vdots & k_N \end{bmatrix} \tag{7}$$

$\{F\}_n = \{F_b(u_b), 0, \dots, 0\}^T$ = non-linear force vector, here $F_b(u_b)$ is the bearing force, which is dependent on u_b.

$\{i\} = \{1, 1, \dots, 1\}$

α_M, α_K = mass and stiffness proportional coefficients of the damping matrix. These coefficients are computed from the damping ratio anchored at the two free vibration modes (Chopra, 2012).

Equation (4) utilizes the Rayleigh damping model, where the damping matrix is defined in terms of the mass and stiffness matrices. In this study, however, the mass-proportional term (α_M) was omitted by setting it to zero. The stiffness-proportional coefficient (α_K) was calculated to achieve a damping ratio of 1% in the isolation mode. The isolation mode was analyzed based on the post-yield stiffness of the isolation system. This stiffness-proportional damping model aligns with the recommendations of Pant et al. (2013).

Dividing both sides of Equation (4) by $m = W/g$, where W is the total weight of the model, yields:

$$[\bar{m}]\{\ddot{u}\} + \left(\alpha_M[\bar{m}] + \alpha_K\left[\bar{k}\right]_C\right)\{\dot{u}\} + \left[\bar{k}\right]_s\{u\} + g\{f\}_n = -[\bar{m}]\{i\}\ddot{u}_g \quad (8)$$

where each element in $[\bar{m}]$ is obtained by dividing the correspondent element in $[M]$ by the total mass m of the model; each element in $\left[\bar{k}\right]_C$ and $\left[\bar{k}\right]_s$ equals the correspondent element in $[K]_C$ and $[K]_s$ divided by m; $\{f\}_n = \{f_b(u_b), 0, .., 0\}^T$, where $f_b(u_b) = F_b(u_b)/W$ is the bearing force normalized by W.

Equations (1-3) (which are used to calculate the stories' shear stiffness) and Equation (8) indicate that the displacement response $\{u\}$ to a specific ground motion u_g does not depend on the absolute mass of the model, but depends on the mass distribution, which is represented by the ratio between m_i and m, provided that the normalized behavior $f_b(u_b)$ of the isolation system is used. For simplicity and to ensure consistent comparison across the very large number of analyzed cases, the mass of the superstructure is assumed to be uniformly distributed over its height, except that the base floor is assigned twice the mass of a typical floor to approximately account for the heavier isolation-level slab commonly found in base-isolated buildings. This idealization, which has been employed in several previous large-scale parametric studies on base-isolated structures (e.g. Kulkarni & Jangid, 2002; Alhan & Sürmeli, 2011), may not fully represent the mass distribution of all real buildings, particularly high-rise structures where column/wall self-weight decreases with height and additional mass is often concentrated at mechanical or transfer levels.

INPUT GROUND MOTIONS

The ground motion records selected for the NIST-11-917-15 project (NEHRP, 2011) were used as the seed motions for this study. These ground motions were selected from the earthquake events with magnitudes larger than 6.0. The site-to-source distance of the records is less than 30 km. The original records in the NIST-11-917-15 project consist of 88 pulse-like motions and 302 non-pulse motions. Detailed information about these records is presented in NEHRP (2011).

To select the motions for this study, the seed motions were further filtered to accept only records with peak ground acceleration (PGA) not smaller than 0.2 g. This additional criterion ensured that only strong records, where base isolation techniques were acknowledged, were considered. As a result, 167 non-pulse records and 78 pulse-like records, totaling 245 records, were used for the numerical analysis.

Figure 2 presents the maximum-direction acceleration response spectra for the selected ground motion records. The maximum-direction spectral acceleration at a specific period was calculated by rotating the ground motion input across all possible angles for a single-degree-of-freedom system, analyzing its response at that period, and identifying the maximum pseudo-acceleration across all orientations. This approach for determining spectral acceleration for each ground motion pair is mandated by ASCE 7-22 (ASCE, 2022).

The graphs in Figure 2 show that the acceleration spectra of the selected motions cover a wide range, thus making it suitable for a general investigation. The graphs also indicate that pulse-like motions are generally stronger than non-pulse motions, especially at the long period range, where isolation systems respond. The difference in the spectra's shape may cause the difference in the effect of the flexibility of the superstructure on the peak displacement of an isolation system. Therefore, this study investigated these motion types separately.

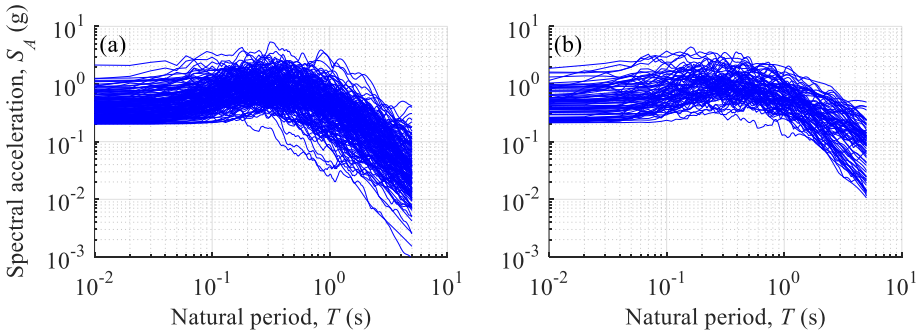

Figure 2. Pseudo spectral acceleration of the selected motions.
a) Non-pulse motions; b) Pulse-like motions

NUMERICAL RESULTS AND DISCUSSION

The numerical simulation for this investigation was performed on 40 isolation systems the sliding friction coefficient of which μ ranged from 0.02 to 0.16 with an increment of 0.02, and the post-yield period T_d ranged from 2.0 s to 6.0 s with an increment of 1.0 s. Each isolation system was applied to a rigid mass system and three building groups the heights of which were one, five, and nine stories. These groups represented low-rise, medium-rise, and high-rise buildings. For each building group, 14 structural systems were investigated. Each structural system corresponded to a fixed-base fundamental period T_1 equal to 1/1.0, 1/1.5,…, 1/5.0, 1/6.0,…, or 1/10 times the effective period T_{eff} of the isolation system with the rigid mass.

To calculate the fundamental period of the fixed-base superstructure, the peak displacement D of the isolation system with the rigid mass model subjected to a ground motion pair was first analyzed. The effective period of the isolation system at the peak displacement was then computed. The fundamental period was then taken as a factor of the effective period. The stories' shear stiffness k_i of the superstructure corresponding to this fundamental period was computed following the instructions in the previous section (i.e., Equations 1-3).

The 40 isolation systems, one rigid mass superstructure, three building groups with 14 structural systems each, and 245 ground motion pairs yielded $40 \times (1 + 3 \times 14) \times 245 = 421{,}400$ non-linear dynamic analyses. The displacement of isolation systems from these analyses was statistically processed and is presented next.

Figure 3 shows the base's displacement trajectories, and Figure 4 plots the normalized hysteretic loops in the maximum-displacement direction of an isolation system in different superstructures subjected to the same ground motion. The motion in consideration was the KJMA motion recorded from the Kobe 1995 earthquake. The isolation system's friction coefficient and post-yield period were 0.06 and 4.0 s, respectively. It should be noted that the envelopes of the hysteretic loops do not precisely follow the unidirectional backbone curve of the isolation system. This is due to its bidirectional coupling behavior, which has been widely observed in past investigations.

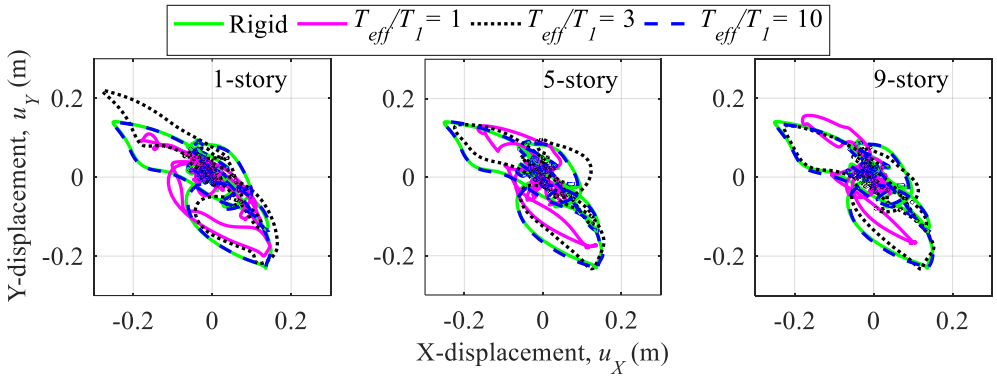

Figure 3. Base's displacement trajectory of an isolation system subjected to the KJMA motion

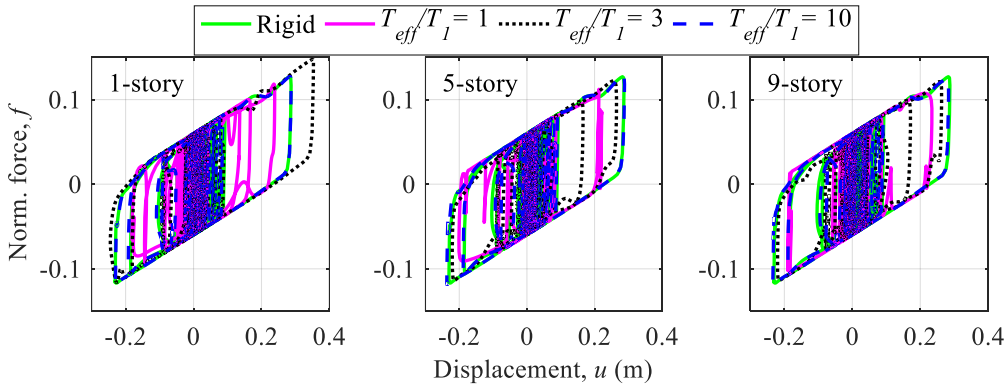

Figure 4. Normalized hysteresis loop in the maxium-displacement direction of an isolation system subjected to the KJMA motion

The results in Figure 3 suggest that the isolation system's response depends not only on the flexibility of

the superstructure, which is represented by the ratio T_{eff}/T_1, but also on the building's height. Interestingly, the maximum-displacement direction for these cases is different, as presented in Table 1, which lists the maximum displacement and the corresponding angle measured from the X-axis. This result indicates that the maximum-displacement direction of an isolation system subjected to a ground motion depends on the flexibility and number of stories of the superstructure.

Table 1. Maximum displacement of an isolation system subjected to the KJMA motion

T_{eff}/T_1	1-story		5-story		9-story	
	Disp. (m)	Angle (deg)	Disp. (m)	Angle (deg)	Disp. (m)	Angle (deg)
∞	0.287	151	0.287	151	0.287	151
1	0.239	-56	0.221	-52	0.234	139
3	0.353	142	0.265	-62	0.263	-62
10	0.287	151	0.289	151	0.283	151

Figure 5 plots the displacement ratio, defined as the ratio of the peak displacement of the isolation system with a flexible superstructure (D_f) to the ratio of the peak displacement of the isolation system with a rigid superstructure (D_r), for all isolated building models subjected to the selected ground motions at different investigated period ratios. Note that for practical application, only data with D_f ranging from 0.05 m to 1.0 m was processed. Each dot in the figure represents the displacement ratio for a single building model subjected to a specific ground motion. The average point (denoted by the x-mark in the figure) at each period ratio represents the average displacement ratio of all individual cases at that period ratio. As expected, the displacement ratio converges to unity when the period ratio is large. At small period ratios, the displacement ratio for individual cases spans wide ranges, meaning that the peak displacement of the isolation system with a very flexible superstructure may vary significantly from that of the isolation system with a rigid superstructure.

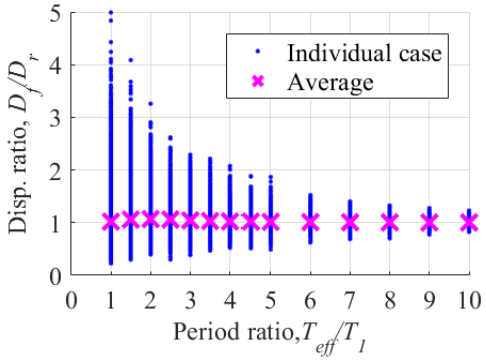

Figure 5. Displacement ratio for all models and all motions

To provide a closer look at the data, Figure 6 presents a bivariate histogram illustrating the frequency distribution as a function of two variables, D_f/D_r and T_{eff}/T_1, and Figure 7 shows the histogram of D_f/D_r at selective period ratios. At period ratios $T_{eff}/T_1 \geq 2$, the high frequency is observed at $D_f/D_r \approx 1.0$, indicating that in most cases, the peak displacement of the isolation system with a flexible structure is comparable to that of the isolation system with a rigid superstructure when the effective period of the isolation system significantly exceeds the superstructure's fundamental period. When $T_{eff}/T_1 < 2$, the frequency peaks at $\frac{D_f}{D_r} < 1.0$, but can spread up to larger than 3.0, meaning that although in most cases, D_f is smaller than D_r, there are cases where it is much larger.

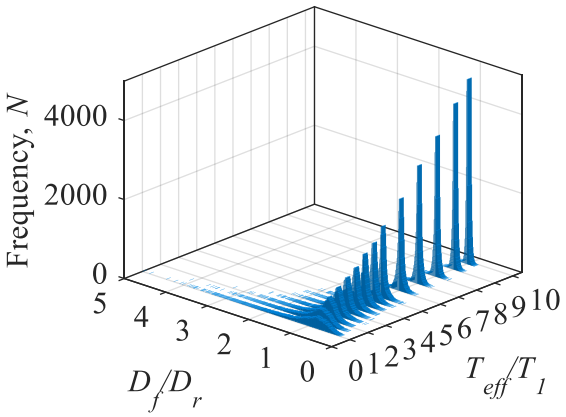

Figure 6. Displacement ratio distribution for all models and motions

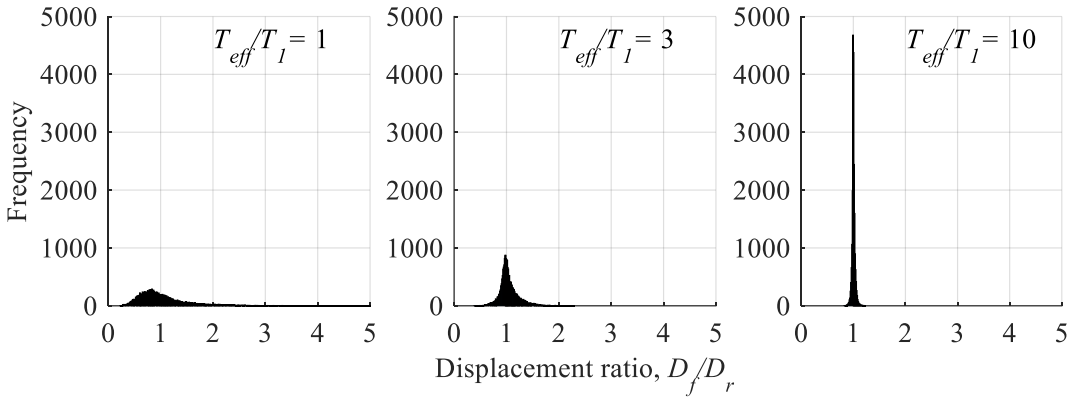

Figure 7. Displacement ratio distribution at selective period ratios

The average displacement ratio and the displacement ratio at selective percentiles for different period ratios are plotted in Figure 8. Note that the average values are the arithmetic means of the data, not the 50th percentile. The 5th percentile and the 95th percentile comprise the mid-90 percent of the data. For example, according to the data, at $T_{eff}/T_1 = 3$, the displacement ratios at the 5th and 95th percentiles are 0.803 and 1.384, respectively, meaning that 90% of the displacement ratios fall between these values.

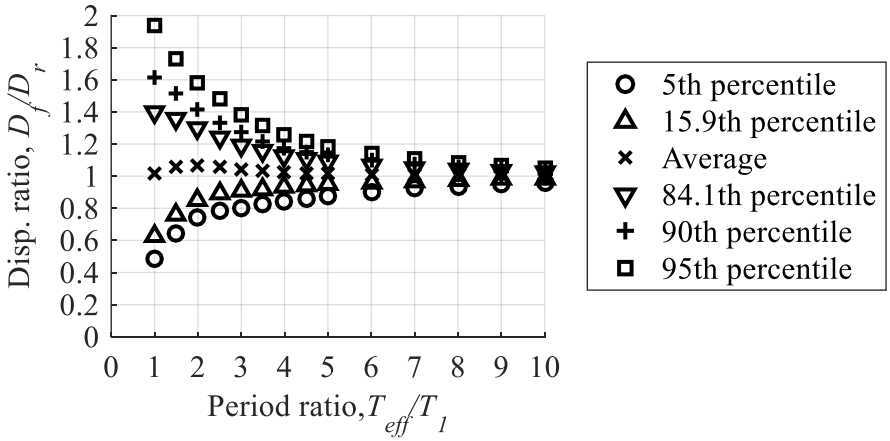

Figure 8. Displacement ratio at selective percentiles for all models and motions

According to the data (which is illustrated in Figure 8), when T_{eff}/T_1 exceeds 2, the average displacement ratios consistently decrease and approach unity. This behavior aligns with the linear theory, which concludes that when the isolation frequency (related to T_{eff}) and the structural frequency (directly related to T_1) are well separated, the influence of higher mode, arising from the superstructure's flexibility, becomes negligible (Kelly, 1990). On average, at $T_{eff}/T_1 = 3$, D_f is 4.3% larger than D_r. With 90% certainty, D_f does not exceed 27.2% D_r when $T_{eff}/T_1 \geq 3$. At this level of certainty, for D_f not to exceed D_r by 10%, the period ratio must be greater than 5.9; and for D_f not to differ from D_r by 10%, T_{eff}/T_1 must not be smaller than 7.3. Table 2 lists the displacement ratio at different percentiles at all investigated period ratios, including these thresholds.

Table 2. Displacement ratio at different percentiles

T_{eff}/T_1	5th percentile	15.9th percentile	Average	84.1th percentile	90th percentile	95th percentile
1	0.487	0.627	1.019	1.401	1.617	1.941
1.5	0.639	0.762	1.059	1.357	1.512	1.732
2	0.745	0.851	1.068	1.298	1.418	1.585
2.5	0.786	0.892	1.06	1.241	1.334	1.479

3	0.803	0.91	1.043	1.191	1.272	1.384
3.5	0.824	0.921	1.032	1.154	1.219	1.315
4	0.841	0.931	1.023	1.126	1.175	1.257
4.5	0.86	0.94	1.02	1.108	1.153	1.219
4.75	*0.867*	*0.943*	*1.018*	***1.1****	*1.142*	*1.201*
5	0.875	0.947	1.016	1.093	1.132	1.183
5.90	*0.899*	*0.958*	*1.012*	*1.071*	***1.1****	*1.144*
6	0.901	0.959	1.011	1.068	1.096	1.139
7	0.921	0.966	1.008	1.052	1.074	1.106
7.27	*0.926*	*0.968*	*1.007*	*1.049*	*1.07*	***1.1****
8	0.937	0.974	1.006	1.041	1.058	1.083
9	0.951	0.979	1.005	1.032	1.046	1.067
10	0.959	0.983	1.004	1.026	1.037	1.054

** These displacement ratios exceed the mean by 10%.*

As commented earlier, pulse-like and no-pulse motions possess different characteristics, and the displacement of an isolation system depends on the number of stories of the superstructure, the relationship between the period ratio and the displacement ratio for different ground motion types and different numbers of stories at selective percentiles were processed and are presented in Figure 9.

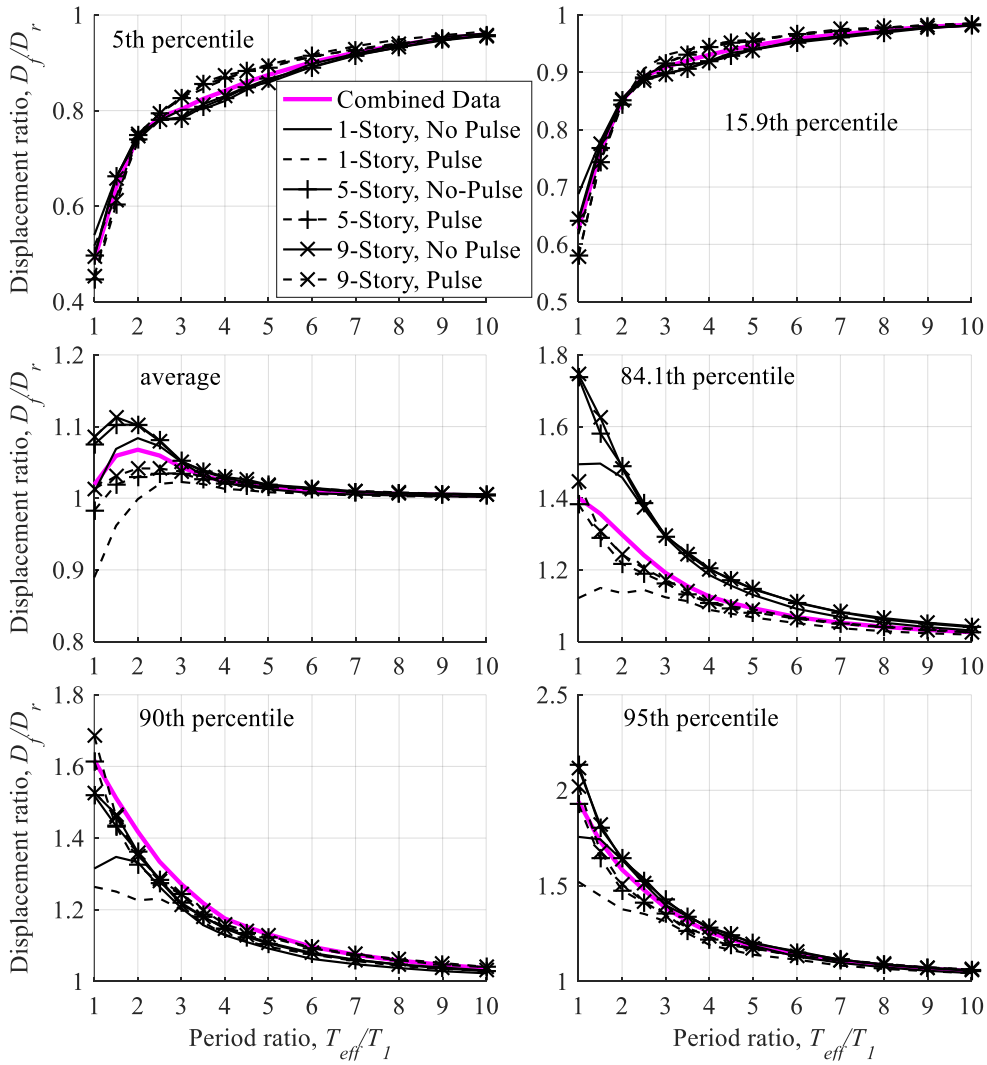

Figure 9. Displacement ratio at selective percentiles for different models and motion types

As expected, the displacement ratio becomes independent of the ground motion type or the number of stories when the period ratio is large. Specifically, for period ratios of 3 or above, the displacement ratio at the selected percentiles for all cases differs from the corresponding displacement ratio of the combined data by less than 5%.

For isolation systems with flexible superstructures, where T_{eff}/T_1 is smaller than 3, the effects of ground motion type and number of stories are prominent. At all investigated percentiles, the displacement ratio for the pulse-like motions is smaller than that of the no-pulse motions. However, at the 5th percentile, the difference between these ratios is not as significant as at other percentiles. These results indicate that the flexibility of the superstructure affects the peak displacement to no-pulse motions more strongly than the peak displacement to pulse-like motions. A similar observation on the effect of the building height shows that the higher the building, the stronger the effect of the structure's flexibility, although they share the same fundamental period. This increased influence may be attributed to the effects of higher modes of vibration and the mass ratio, defined as the ratio of the floor mass to the total mass, as highlighted in previous studies (Kelly, 1990; Kulkarni & Jangid, 2003).

CONCLUSIONS

This study investigated the impact of superstructure flexibility on the peak displacement of isolation systems with single friction pendulum (SFP) bearings under seismic excitation. By analyzing a wide range of isolation systems and ground motions, the relationship between the flexibility of the superstructure, represented by the period ratio T_{eff}/T_1, and the isolation system's response was quantified. Key findings highlight the critical role of superstructure flexibility in determining peak displacement:

1. When $T_{eff}/T_1 > 2$, the displacement ratio D_f/D_r stabilizes near unity, indicating that the isolation system's response becomes largely independent of the superstructure's flexibility. For example, at $T_{eff}/T_1 = 3$, the average displacement ratio is 1.043, with 90% of cases falling between 0.803 and 1.384. Current design standards, such as ASCE 7-2022 and Eurocode 8, adopt a T_{eff}/T_1 threshold of 3 to justify the rigid superstructure assumption. While this is sufficient on average, the results suggest that higher thresholds are necessary for more reliable predictions. For practical purposes, ensuring that D_f does not exceed D_r by more than 10% with 90% certainty requires $T_{eff}/T_1 > 5.9$, while limiting the difference to within ±10% requires $T_{eff}/T_1 > 7.3$.
2. When $T_{eff}/T_1 < 2$, the displacement ratio exhibits significant variability, ranging from less than 0.3 to over 3.0. This underscores the pronounced influence of superstructure flexibility on the peak displacement. In this range, higher modes of vibration and mass ratios play a critical role in amplifying or reducing the displacement response.
3. The effects of ground motion type and building height were also investigated. For $T_{eff}/T_1 \geq 3$, the displacement ratios remain consistent across pulse-like and no-pulse motions and across different building heights, with deviations of less than 5% from the combined data. However, when $T_{eff}/T_1 < 3$, significant differences emerge: pulse-like motions result in lower displacement ratios compared to no-pulse motions, and taller buildings exhibit stronger effects of superstructure flexibility, despite having the same fundamental period.

Acknowledgements

This work was supported by the Industrial University of Ho Chi Minh City for this research project under Grant No. 23.1XD04. The authors are grateful for this generous financial support.

REFERENCES

Alhan, C., & Sürmeli, M. (2011). Shear building representations of seismically isolated buildings. *Bulletin of Earthquake Engineering*, *9*(5), 1643-1671. https://doi.org/10.1007/s10518-011-9293-z

Alici, F.S., Sucuoglu, H., & Ozcamur, U. (2024). A critical assessment of the design displacements of friction pendulum systems. *Soil Dynamics and Earthquake Engineering*, *177*, 108426. https://doi.org/10.1016/j.soildyn.2023.108426

American Society of Civil Engineers (ASCE). (2022). *ASCE/SEI 7-22 Minimum design loads and associated criteria for buildings and other structures.* Reston, VA, USA: ASCE.

Bhagat, S., & Wijeyewickrema, A.C. (2017). Seismic

response evaluation of base-isolated reinforced concrete buildings under bidirectional excitation. *Earthquake Engineering and Engineering Vibration*, *16*(2), 365-382. https://doi.org/10.1007/s11803-017-0387-8

Buckle, I. G., & Mayes, R. L. (1990). Seismic isolation: history, application, and performance: A world view. *Earthquake Spectra*, *6*(2), 161-201. https://doi.org/10.1193/1.1585564

Cardone, D., Gesualdi, G., & Brancato, P. (2015). Restoring capability of friction pendulum seismic isolation systems. *Bulletin of Earthquake Engineering*, *13*(8), 2449-2480. https://doi.org/10.1007/s10518-014-9719-5

Chopra, A. (2012). *Dynamics of structures* (4th Edn.). New York: Prentice Hall.

Cilsalar, H., & Constantinou, M.C. (2017). Effect of vertical ground motion on the response of structures isolated with friction pendulum isolators. *International Journal of Earthquake and Impact Engineering*, *2*(2), 135. https://doi.org/10.1504/IJEIE.2017.089048

Constantinou, M.C., Tsopelas, P., Kim, Y.S., & Okamoto, S. (1993). Experimental and analytical study of a friction pendulum system (FPS). *NCEER Report*, 93-0020.

Dao, N.D., Ryan, K.L., & Nguyen-Van, H. (2019). Evaluating simplified models in predicting global seismic responses of a shake table-test building isolated by triple friction pendulum bearings. *Earthquake Engineering & Structural Dynamics*, *48*(6), 594-610. https://doi.org/10.1002/eqe.3152

Dao, N.D., Nguyen-Van, H., Nguyen, T.H.A., & Chung, A. B. (2020). A new statistical equation for predicting non-linear time history displacement of seismic isolation systems. *Structures*, *24*, 177-190. https://doi.org/10.1016/j.istruc.2020.01.019

Dao, N.D. (2025). Equations and artificial neural network models for predicting displacement of lead rubber isolation systems. *Structures*, *78*, 109242. https://doi.org/10.1016/j.istruc.2025.10924

Dao, N.D. (2026). Formulae for predicting the peak dynamic displacement of isolation systems with single friction pendulum bearings. *Soil Dynamics and Earthquake Engineering*, *200*, 109905. https://doi.org/10.1016/j.soildyn.2025.109905

Dicleli, M., & Buddaram, S. (2007). Comprehensive evaluation of equivalent linear analysis method for seismic-isolated structures represented by SDOF systems. *Engineering Structures*, *29*(8), 1653-1663. https://doi.org/10.1016/j.engstruct.2006.09.013

Dolce, M., Cardone, D., & Croatto, F. (2005). Frictional behavior of steel-PTFE interfaces for seismic isolation. *Bulletin of Earthquake Engineering*, *3*(1), 75-99. https://doi.org/10.1007/s10518-005-0187-9

European Committee for Standardization (CEN). (2004). *Eurocode 8: design of structures for earthquake resistance - Part 1: General rules, seismic actions and rules for buildings.* Brussels, Belgium: CEN.

Fadi, F., & Constantinou, M.C. (2010). Evaluation of simplified methods of analysis for structures with triple friction pendulum isolators. *Earthquake Engineering & Structural Dynamics*, *39*(1), 5-22. https://doi.org/10.1002/eqe.930

Fenz, D.M., & Constantinou, M.C. (2008). *Development, implementation and verification of dynamic analysis models for multi-spherical sliding bearings*. Multidisciplinary Center for Earthquake Engineering Research, State University of New York at Buffalo.

Jamalvandi, M., & Amiri, M. (2021). Influence of seismic isolation systems on behavior of fluid inside thin-walled steel tanks. *Jordan Journal of Civil Engineering, 15*(4), 534-550.

Jing, W., & Zhang, Y. (2024). Seismic responses of large height-width ratio liquid storage structure with base isolation and baffles. *Jordan Journal of Civil Engineering, 18*(3), 419-435. https://doi.org/10.14525/JJCE.v18i3.05

Kanbir, Z., Alhan, C., & Özdemir, G. (2020). Influence of superstructure modeling approach on the response prediction of buildings with LRBs considering heating effects. *Structures*, *28*, 1756-1773. https://doi.org/10.1016/j.istruc.2020.09.061

Katsaras, C.P., Panagiotakos, T.B., & Kolias, B. (2008). Restoring capability of bilinear hysteretic seismic isolation systems. *Earthquake Engineering & Structural Dynamics*, *37*(4), 557-575. https://doi.org/10.1002/eqe.772

Kelly, J.M. (1986). Aseismic base isolation: Review and bibliography. *Soil Dynamics and Earthquake Engineering, 5*(4), 202-216. https://doi.org/10.1016/0267-7261(86)90006-0

Kelly, J.M. (1990). Base isolation: Linear theory and design. *Earthquake Spectra*, *6*(2), 223-244. https://doi.org/10. 1193/1.1585566

Kim, H., & Constantinou, M.C. (2024). Testing seismic isolators for the effect of maximum earthquake based

on measure of cumulative energy. *Earthquake Engineering & Structural Dynamics*, *53*(12), 3924-3937. https://doi.org/10.1002/eqe.4202

Kulkarni, J.A., & Jangid, R.S. (2002). Rigid body response of base-isolated structures. *Journal of Structural Control*, *9*(3), 171-188. https://doi.org/10.1002/stc.11

Kulkarni, J.A., & Jangid, R.S. (2003). Effects of superstructure flexibility on the response of base-isolated structures. *Shock and Vibration*, *10*(1), 1-13. https://doi.org/10.1155/2003/368693

Mokha, A., Constantinou, M., & Reinhorn, A. (1988). *Teflon bearings in aseismic base isolation: Experimental studies and mathematical modeling.* State University of New York, Buffalo. Buffalo: National Center for Earthquake Engineering Research.

Mokha, A., Constantinou, M., & Reinhorn, A. (1990). *Experimental study and analytical prediction of earthquake response of a sliding isolation system with a spherical surface.* State University of New York at Buffalo. Buffalo: National Center for Earthquake Engineering Research.

National Earthquake Hazards Reduction Program (NEHRP) Consultants JointVenture. (2011). *Selecting and scaling earthquake ground motions for performing response-history analyses (NIST GCR 11-917-15).* Redwood, CA, USA: NEHRP Consultants Joint Venture.

Nguyen, N.V., Nguyen, H.D., & Dao, N.D. (2022). Machine learning models for predicting maximum displacement of triple pendulum isolation systems. *Structures*, *36*, 404-415. https://doi.org/10.1016/j.istruc.2021.12.024

Nhan, D.D., & Ai, C.B. (2020). A constant friction coefficient model for concave friction bearings. *Journal of Science and Technology in Civil Engineering (STCE) - NUCE*, *14*(1), 112-126. https://doi.org/10.31814/stce.nuce2020-14(1)-10

Pant, D.R., Wijeyewickrema, A.C., & ElGawady, M.A. (2013). Appropriate viscous damping for non-linear time-history analysis of base-isolated reinforced concrete buildings. *Earthquake Engineering & Structural Dynamics*, *42*(15), 2321-2339. https://doi.org/10.1002/eqe.2328

Peng, P., Dongbin, Z., Yi, Z., Yachun, T., & Xin, N. (2018). Development of a tunable friction pendulum system for semi-active control of building structures under earthquake ground motions. *Earthquake Engineering & Structural Dynamics*, *47*(8), 1706-1721. https://doi.org/10.1002/eqe.3036

Quaglini, V., Dubini, P., & Poggi, C. (2012). Experimental assessment of sliding materials for seismic isolation systems. *Bulletin of Earthquake Engineering*, *10*(2), 717-740. https://doi.org/10.1007/s10518-011-9308-9

van de Lindt, J.W., & Jiang, Y. (2014). Empirical selection equation for friction pendulum seismic isolation bearings applied to multistory woodframe buildings. *Practice Periodical on Structural Design and Construction*, *19*(3). https://doi.org/10.1061/(ASCE)SC.1943-5576.0000198

Xu, Y., Guo, T., & Yan, P. (2019). Design optimization of triple friction pendulums for base-isolated high-rise buildings. *Advances in Structural Engineering*, *22*(13), 2727-2740. https://doi.org/10.1177/1369433219849840

Zhong, J., Zhu, Y., Zheng, X., & Han, Q. (2023). Multi-variable probabilistic seismic demand models for parametric fragility prediction of isolated bridges portfolios under pulse-like GMs. *Engineering Structures*, *292*, 116517. https://doi.org/10.1016/j.engstruct.2023.116517